

LaMamba-Diff: Linear-Time High-Fidelity Diffusion Models Based on Local Attention and Mamba

Yunxiang Fu Chaoqi Chen Yizhou Yu
The University of Hong Kong

yunxiang@connect.hku.hk, cqchen1994@gmail.com, yizhouy@acm.org

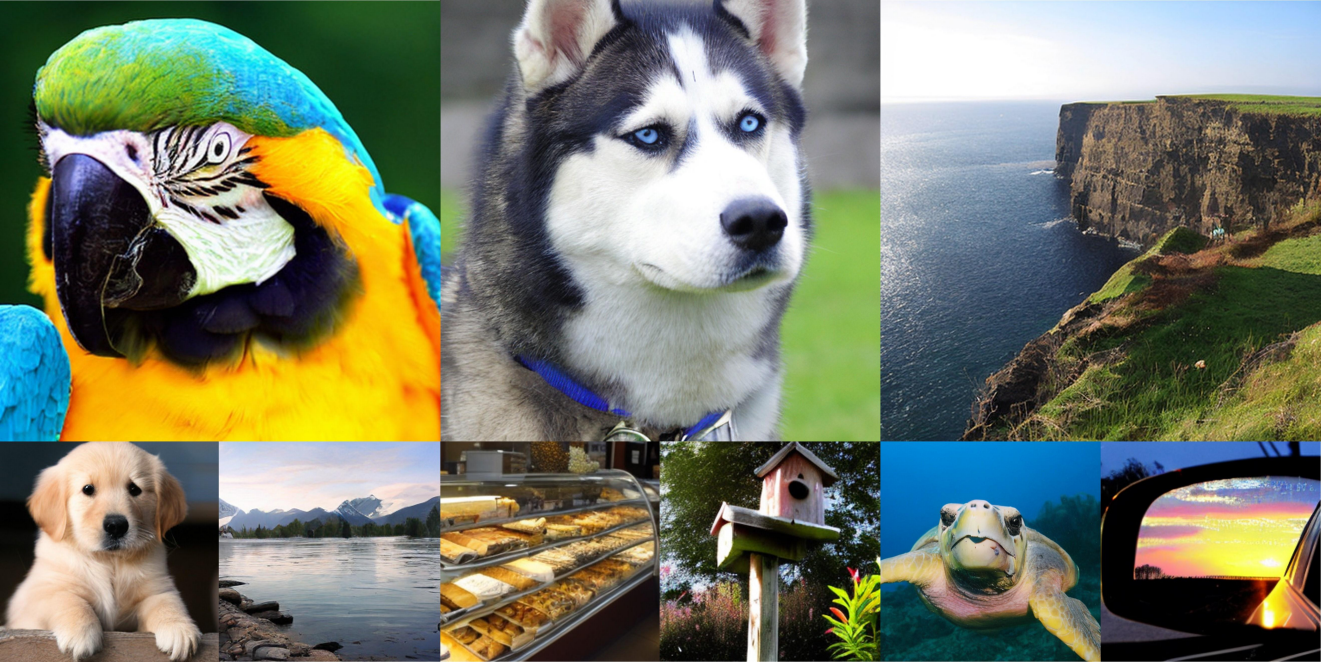


Figure 1. Sample images generated by our model trained on ImageNet at 512x512 and 256x256 resolutions.

Abstract

Recent Transformer-based diffusion models have shown remarkable performance, largely attributed to the ability of the self-attention mechanism to accurately capture both global and local contexts by computing all-pair interactions among input tokens. However, their quadratic complexity poses significant computational challenges for long-sequence inputs. Conversely, a recent state space model called Mamba offers linear complexity by compressing a filtered global context into a hidden state. Despite its efficiency, compression inevitably leads to information loss of fine-grained local dependencies among tokens, which are crucial for effective visual generative modeling. Motivated by these observations, we introduce Local Attentional Mamba (LaMamba) blocks that combine the strengths of self-attention and Mamba, capturing both global contexts and local details with linear complexity. Leveraging the efficient U-Net architecture, our model exhibits exceptional

scalability and surpasses the performance of DiT across various model scales on ImageNet at 256x256 resolution, all while utilizing substantially fewer GFLOPs and a comparable number of parameters. Compared to state-of-the-art diffusion models on ImageNet 256x256 and 512x512, our largest model presents notable advantages, such as a reduction of up to 62% GFLOPs compared to DiT-XL/2, while achieving superior performance with comparable or fewer parameters. Our code is available at <https://github.com/yunxiangfu2001/LaMamba-Diff>.

1. Introduction

Diffusion models have made significant strides in the field of generative modeling [21, 52], especially for images [8, 34, 39–41, 45], often surpassing the previously popular generative adversarial networks (GANs) [12]. The advancements of diffusion models have been driven by many or-

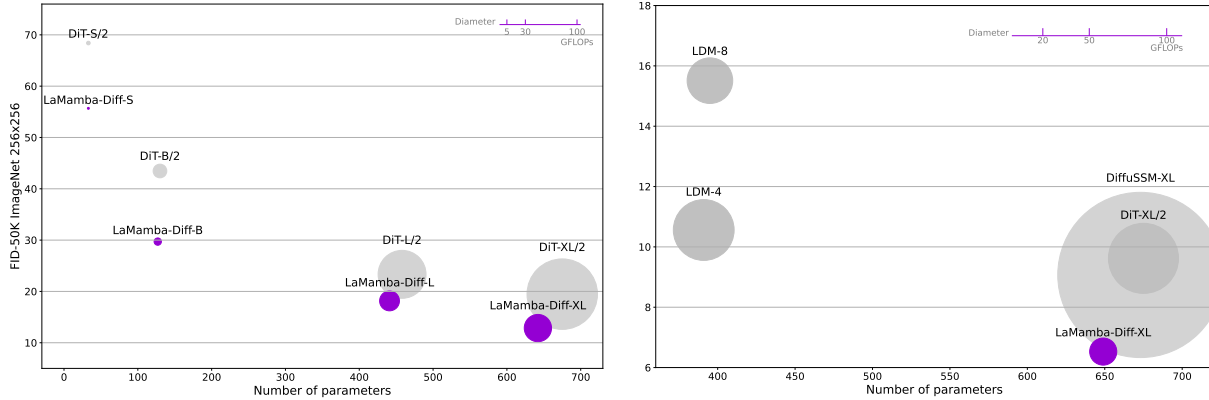


Figure 2. Unconditional image generation quality on ImageNet 256x256. The area of bubbles denote GFLOPs. *Left*: FID-50K of LaMamba-Diff models trained for 400k iterations. Performance improves with the number of parameters and GFLOPs. *Right*: Our largest model outperforms state-of-the-art diffusion models with substantially fewer GFLOPs.

thogonal factors, including sampling approaches [20, 21, 25, 51], latent space modeling [41], and backbone architecture designs [37, 55]. Despite recent attempts to devise innovative backbones, state-of-the-art backbones for diffusion models [24, 37, 41] largely rely on self-attention [54] for high-fidelity generation. The effectiveness of self-attention stems from its capacity to accurately capture global contexts and fine-grained local dependencies from inputs by explicitly computing all-pair interactions among input tokens. However, their quadratic computational complexity with respect to the input sequence length poses computational challenges when dealing with long sequences, such as high-resolution images or sequences formed with a small patch size.

To address the quadratic complexity of self-attention, a recent state space model (SSM) named Mamba [14] has been proposed. Using dynamic weights, Mamba captures global contexts with linear time by compressing contextual information of input tokens into a hidden state. Demonstrating a strong potential in long-sequence modeling, Mamba has been applied across diverse domains, including medical data [28, 43], point clouds [29], and vision tasks [30, 58]. However, unlike self-attention, the compression and selective process of Mamba does not explicitly compute pairwise interactions. Consequently, part of fine-grained local information is lost, leading to sub-optimal performance. The significance of local details for generative modeling is demonstrated by the detrimental decline in the performance of DiT [37] as the patch size increases, attributed to the loss of fine-grained information within each patch [18].

In light of these observations, we introduce a novel Local Attentional Mamba (LaMamba) block that combines the strengths of Transformers and Mamba to accurately model global contexts and local details with linear complexity. LaMamba captures global contexts efficiently using Mamba

while accurately preserving fine-grained local dependencies using local self-attention. Our local self-attention has linear complexity by computing pairwise interactions within a context window with a fixed size. LaMamba brings the best of two worlds for visual generative modeling, offering favorable properties like scalability, robustness, and efficiency.

Based on LaMamba blocks, we design LaMamba-Diff, a novel backbone for diffusion models that adopts a U-Net architecture [42]. LaMamba-Diff naturally constructs multi-scale hierarchical features through down and up-sampling and exhibits efficiency by compressing spatial dimensions during the downsampling phase. The highly efficient design of LaMamba and LaMamba-Diff allows us to utilize 1×1 patches, which enables more accurate modeling of fine-grained spatial dependencies by preventing the loss of local details within each patch [18]. In particular, with a comparable number of parameters, LaMamba-Diff with a patch size of 1 uses significantly fewer GFLOPs compared to DiT [37] with a patch size of 2, despite that DiT has a 4x shorter input sequence length.

We evaluate the performance of LaMamba-Diff on the widely-used ImageNet dataset for image generation. As illustrated in Fig. 2 (right), LaMamba-Diff achieves state-of-the-art Fréchet Inception Distance (FID) with comparable or fewer parameters and significantly less GFLOPs on ImageNet at 256×256 resolution. Moreover, as depicted in Fig. 2 (left), LaMamba-Diff exhibits excellent scalability with FID scores consistently decreasing with the number of parameters and GFLOPs. In the class-conditional ImageNet 256x256 image generation benchmark, LaMamba-Diff-XL achieves a state-of-the-art FID of 2.04 using 57.6% fewer GFLOPs compared to DiT-XL/2. For class-conditioned ImageNet 512x512 image generation, LaMamba-Diff-XL achieves an FID of 3.01 using 61.6% fewer GFLOPs com-

pared to DiT-XL/2. These results demonstrate the effectiveness and efficiency of LaMamba-Diff for high-resolution image generation tasks.

To summarise, our contributions in this paper are three-fold:

- We design a novel LaMamba block that combines the strengths of Transformers and Mamba, accurately capturing global contexts and local details with linear complexity.
- We propose LaMamba-Diff, a highly efficient backbone for diffusion models. LaMamba-Diff allows a patch size of 1 without substantial computational overhead, which was previously unavailable for diffusion backbones.
- Experimental results demonstrate that LaMamba-Diff achieves state-of-the-art FID using significantly fewer GFLOPs. Additionally, LaMamba-Diff demonstrates excellent scalability.

2. Related works

Diffusion model backbones. Diffusion models (DM) belong to a class of probabilistic generative models that iteratively corrupt data by introducing noise through a forward process, and subsequently learn to reverse this process for sample generation [21, 50, 53]. Recently, DM has become the de facto choice for image generation, due to its capability to generate photo-realistic images and stable training property [7, 39, 39, 41, 41, 45, 57], which was unavailable for the previous state-of-the-art GANs [12]. The backbones for state-of-the-art DM are UNet-based [21, 41] or Transformer-based [37] and rely heavily on attention [54]. However, the quadratic complexity of attention hinders the application of diffusion models to long sequential data. Very recently, to achieve linear complexity, state space models have been leveraged to construct backbones for DM [10, 22, 55] by replacing the self-attention module in existing backbones like DiT [37] with Mamba [14]. However, they fail to outperform DiT using a comparable number of parameters and GFLOPs. In contrast, we propose a hybrid Mamba backbone using local attention, achieving linear complexity without sacrificing image fidelity and outperforming DiT using fewer GFLOPs and parameters.

State space models. A recent state space model named Mamba [14] has gained popularity in sequence modeling renowned for its linear complexity, dynamic weights, and global receptive field. Mamba has been widely explored in various domains, including vision backbones [30, 58], medical imaging [28, 43], 3D point clouds [29], tabular data [1], and image/video generation [10, 22, 36, 55]. In this paper, we investigate the use of Mamba for image generation, distinguishing ourselves from previous works by utilizing local attention to address the issue of fine-grained local detail loss when replacing attention with Mamba. Concurrently, the Matten model [11] explores different combina-

tions of Mamba and attention for video generation using an isotropic architecture, but exhibits quadratic complexity with sequence lengths. In contrast, our work has linear complexity and employs an efficient U-Net architecture that permits a patch size of 1, thereby avoiding the loss of local information within patches [18].

3. Preliminary

Latent diffusion models (LDMs) [41] typically operate on the latent space of a pre-trained variational autoencoder (VAE) [9, 26]. The pre-trained VAE encoder \mathcal{E} is used to transform data samples $x_0 \sim p_{data}(x)$ into latent representation $z_0 = \mathcal{E}(x_0)$ with a downsampling factor of 8. LDMs learn to sample from this latent distribution by progressively perturbing z in a forward process, and then learn to reverse this process. Specifically, forward diffusion gradually convert z_0 to a prior noise distribution with intermediate noisy latents z_1, \dots, z_T and $z_T \sim \mathcal{N}(0, \mathbf{I})$ by applying Gaussian transitions: $q(z_t|z_{t-1}) = N(z_t; \sqrt{1 - \beta_t}z_{t-1}, \beta_t\mathbf{I})$, where $t \in \{1, \dots, T\}$ denote the timestep and $\beta_t \in (0, 1)$ is a pre-defined noise variance hyperparameter.

LDMs are trained to learn the reverse diffusion process $p_\theta(z_{t-1}|z_t) = \mathcal{N}(z_{t-1}; \mu_\theta(z_t), \Sigma_\theta(z_t))$, where mean $\mu_\theta(z_t)$ and variance $\Sigma_\theta(z_t)$ are parameterized by neural networks. In practice, the variance Σ_θ can be predefined or learned, and the mean μ_θ is parameterized using a noise predictor ϵ_θ [21, 35]. The training loss can be rewritten as a simplified form of the variational lower bound [26] $\mathcal{L}_{simple} = \sum_{t=1}^{T-1} \mathbb{E}_{z_0, \epsilon} [\|\epsilon_t - \epsilon_\theta(z_t, t)\|^2]$ [35]. Additionally, we follow the common practice to train Σ_θ using \mathcal{L}_{vlb} [35, 37]. After training, novel latents z_0 can be sampled by iteratively denoising a random noise z_T using the noise predicted by ϵ_θ with $z_{t-1} \sim p_\theta(z_{t-1}|z_t)$ via the reparameterization trick. Subsequently, images are generated by passing z_0 to the pre-trained VAE decoder. We follow LDMs by training diffusion models in the latent space of a pre-trained VAE.

State space models (SSM) [14–16, 49] are sequence-to-sequence models that map input signals $x(t) \in \mathbb{R}$ to output signals $y(t) \in \mathbb{R}$ through a latent $h(t) \in \mathbb{R}^{N \times 1}$. The continuous time process for a linear time-invariant (LTI) SSM can be formulated as

$$\begin{aligned} h'(t) &= Ah(t) + Bx(t), \\ y(t) &= Ch(t) + \bar{D}x(t), \end{aligned} \quad (1)$$

where $A \in \mathbb{R}^{N \times N}$, $B \in \mathbb{R}^{N \times 1}$, $C \in \mathbb{R}^{1 \times N}$ denote the diagonal state matrix, input matrix, and output matrix for hidden size N , respectively, and $\bar{D} \in \mathbb{R}$ is a shortcut that provides a direct path from input to y .

In order to utilize SSM with real-world data, which is typically discrete, the continuous process represented in Equation (1) is discretized using the zero-order hold (ZOH)

rule, which is formulated as [17]

$$\begin{aligned} h_t &= \bar{A}h_{t-1} + \bar{B}x_t, \\ y_t &= Ch_t + \bar{D}x_t, \end{aligned} \quad (2)$$

where $\bar{A} = e^{(\Delta A)}$ and $\bar{B} = (\Delta A)^{-1}(e^{(\Delta A)} - I) \cdot (\Delta B)$ with Δ as the timescale parameter for ZOH.

Mamba [14] relaxes the LTI constraint and introduces a selective scan mechanism (S6) that allows hidden states h to be contextually aware of the input using dynamic weights. Specifically, S6 introduces selectivity to Δ, B , and C , enabling them to capture the context of input tokens, while the context of \bar{A} is obtained from Δ . Given an input $x_t \in \mathbb{R}^D$ with D channels, S6 independently selects the context of each channel, and compresses the selected context for each channel into a hidden state $h \in \mathbb{R}^N$, with N representing the SSM state dimension. Our proposed model builds on the strengths of Mamba, leveraging its ability to capture global contextual information in linear time, while also addressing the loss of fine-grained details through the incorporation of local attention.

4. Methodology

We present a novel linear-time hybrid U-Net architecture named Local Attentional Mamba for Diffusion (LaMamba-Diff). LaMamba-Diff, built upon Local Attentional Mamba (LaMamba) blocks, is designed to combine the strengths of Mamba and self-attention, having dynamic weights that efficiently capture global contexts while precisely modeling local dependencies. Fig.3 provides an illustration of LaMamba-Diff.

4.1. LaMamba blocks

Overview. Transformers have demonstrated remarkable performance as backbones in the latent diffusion framework [37, 41]. The effectiveness of Transformers can be attributed to self-attention, which is capable of capturing detailed contextual information from all input token pairs. However, the quadratic complexity of self-attention with respect to the length of the input sequence poses scalability challenges for long input sequences arising from high-resolution scenarios or small patch sizes. In contrast, Mamba [14] recurrently compresses contextual information of an input sequence into a single hidden state to achieve linear time complexity. However, this approach inevitably suffers from a loss of detailed information in input tokens due to compression. However, such detailed information is crucial to visual generative modeling. This limitation is evident in performance comparisons between SSM-based diffusion models and DiT, where the former fails to outperform the latter when using a comparable number of parameters and GFLOPs [10, 37, 55]. To bring the best of both worlds, we

introduce Local Attentional Mamba (LaMamba) blocks that capture both global contexts and local details in linear time.

Our proposed LaMamba block is illustrated in Fig. 3 (right) and consists of three components: a visual state space model (VSSM), a local attention module, and a feed-forward network (FFN). Every component is equipped with a residual connection. Additionally, every component integrates condition information, such as timesteps and class labels, using adaptive layer normalization (AdaLN) [8] and a scaling operation before the residual connection. The VSSM is a variation of the original Mamba block tailored for 2D visual data [30] and is used to efficiently capture global contexts. We adopt spatially continuous scans in four complementary directions [56]. Local attention explicitly computes local pairwise attentions among input tokens without compression, resulting in fine-grained local representations. The standard FFN with a hidden dimension expansion ratio of 4 is added at the end of the block. LaMamba integrates conditions using AdaLN, where the scale and shift parameters (γ and β) of Layer Normalization [2] are regressed from the condition embedding using a multi-layer perceptron (MLP). Additionally, a dimension-wise scaling operation is adopted for zero-initialization [13, 37], where the MLP is initialized to make the scaling parameter (α) a zero-vector at the start of training. This makes the LaMamba block an identity function initially as the output of each component is equal to its residual connection. As the visual state space model (VSSM), local attention module, and feed-forward network (FFN) all exhibit linear time complexity, LaMamba also maintains linear time complexity. Furthermore, the computational cost associated with adaptive layer normalization (AdaLN) and zero-initialization is negligible in terms of GFLOPs.

Main components. Originally designed for sequence modeling in natural language processing, Mamba casually processes 1D input sequences. Directly applying Mamba to non-casual 2D visual signals may yield sub-optimal results as it does not consider 2D spatial information, which is crucial for vision tasks [30, 58]. Hence, we adopt a visual state space module (VSSM) that explicitly models 2D spatial information. We explore four variants of VSSM: (1) Bi-directional Mamba (ViM) [58] adds positional embeddings and performs both forward and backward scanning to incorporate spatial information. (2) LocalVMamba [23] partitions input tokens into windows, each of which is scanned individually to ensure local spatial information is encoded closely together. Afterwards, a global scan is carried out across windows. (3) EfficientVMamba [38] implements multiple scanning paths efficiently by scanning tokens with a fixed step size larger than one and aggregating the results along different scanning paths. This approach allows tokens to integrate information from multiple scanning directions without introducing computational overhead. (4)

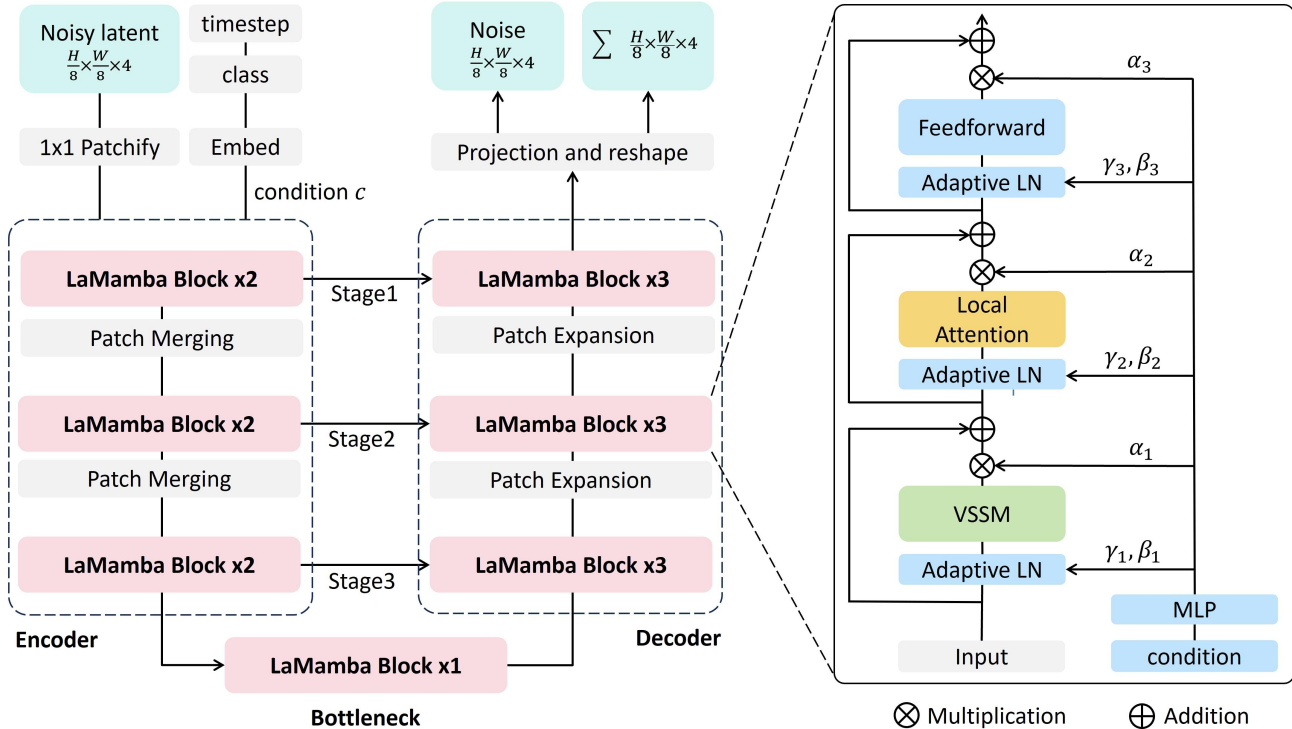


Figure 3. Network architecture of LaMamba-Diff. *Left*: Architecture of LaMamba-Diff-S. *Right*: Local attentional Mamba block.

2D Selective-Scan (SS2D) blocks [30] adopt four distinct and complementary scanning paths, enabling each token to integrate information from all other tokens in four different directions. Moreover, SS2D removes the multiplicative branch in original Mamba blocks [14]. We modify the scanning trajectories in SS2D to spatial continuous scans [56]. Unless otherwise stated, all models in this work use our modified SS2D block as the VSSM owing to its superior performance, as shown in the ablation study presented in Table 6.

The compression and selection mechanism in VSSM serves to filter out irrelevant information for improved efficiency [14] but may lose information about fine-grained local details and dependencies. To address this issue, we incorporate a local attention module for fine-grained local representations. In practice, we utilize window-based attention [31], where the input is partitioned into non-overlapping square windows and self-attention is computed within each window to explicitly capture local dependencies without compression. Note that complexity is linear with respect to sequence length because the size of every window is fixed and hence the number of tokens within every window is a constant.

To integrate conditions into diffusion models, we follow the widespread usage of AdaLN [8, 37]. Concretely, we replace layer normalization [2] with AdaLN by regressing

the scale and shift parameters (γ and β) using the sum of the embedding vectors of timestep t and class label l . This process can be formulated as $\text{AdaLN}(h, c) = \gamma \text{LN}(h) + \beta$, where γ and β are computed by passing the conditioning embedding c to an MLP.

Summary. The novelty of LaMamba lies in the composition of Mamba and local attention modules to complement each other within each block. Despite that LaMamba is based on VSSM [30] and windowed local attention [31], to the best of our knowledge, this is the first attempt to incorporate both Mamba and local attention within the building block of a diffusion model backbone, resulting in the capability to capture both global contexts and fine-grained local details with linear time complexity. LaMamba naturally inherits the strengths of both Transformer and Mamba, including scalability, robustness, and efficiency. This is demonstrated by the state-of-the-art performance and scalability analysis on ImageNet, as shown in Table 3 and Figure 2, respectively. Moreover, ablation studies in Table 5 empirically confirm the effectiveness of local attention in learning fine-grained local representations.

4.2. Network architecture

The inherent hierarchical structure observed in natural images [47] motivates the adoption of hierarchical models for image generation [21, 41]. This approach has proven

	Stage	Output size	Small	Base	Large	X-Large
Encoder	1	16×16	[LaMamba] $\times 2$ (96) Patch Merge (192)	[LaMamba] $\times 2$ (192) Patch Merge (384)	[LaMamba] $\times 2$ (256) Patch Merge (512)	[LaMamba] $\times 2$ (320) Patch Merge (640)
	2	8×8	[LaMamba] $\times 2$ (192) Patch Merge (384)	[LaMamba] $\times 2$ (384) Patch Merge (768)	[LaMamba] $\times 2$ (512) Patch Merge (1024)	[LaMamba] $\times 2$ (640) Patch Merge (1280)
	3	8×8	[LaMamba] $\times 2$ (384)	[LaMamba] $\times 2$ (768)	[LaMamba] $\times 2$ (1024)	[LaMamba] $\times 2$ (1280)
	4	8×8	Identity (384)	Identity (768)	[LaMamba] $\times 2$ (1024)	[LaMamba] $\times 2$ (1280)
Bottleneck	-	8×8	[LaMamba] $\times 1$ (384)	[LaMamba] $\times 1$ (768)	[LaMamba] $\times 2$ (1024)	[LaMamba] $\times 2$ (1280)
Decoder	4	8×8	Identity (384)	Identity (768)	[LaMamba] $\times 3$ (1024)	[LaMamba] $\times 3$ (1280)
	3	8×8	[LaMamba] $\times 3$ (384)	[LaMamba] $\times 3$ (768)	[LaMamba] $\times 3$ (1024)	[LaMamba] $\times 3$ (1280)
	2	16×16	Patch Expand (192) [LaMamba] $\times 3$ (192)	Patch Merge (384) [LaMamba] $\times 3$ (384)	Patch Merge (512) [LaMamba] $\times 3$ (512)	Patch Merge (640) [LaMamba] $\times 3$ (640)
	1	32×32	Patch Expand (96) [LaMamba] $\times 3$ (96)	Patch Merge (192) [LaMamba] $\times 3$ (192)	Patch Merge (256) [LaMamba] $\times 3$ (256)	Patch Merge (320) [LaMamba] $\times 3$ (320)
Output layer	-	32×32	adaLN - ζ Linear (8)			
Param	-	-	32M	127M	449M	656M
GFLOPs	-	-	3.19	12.32	33.39	49.90

Table 1. Summary of LaMamba-Diff network architectures. The noisy latent produced from all our networks is shaped 32×32 , which corresponds to 256×256 input images. The hidden dimensions of each block are shown in brackets.

successful in the U-Net architecture, which naturally constructs multi-scale hierarchical representations, commonly used for diffusion models [21, 41, 42], but not for diffusion Transformers [4, 37]. To leverage hierarchical features and improve efficiency, we adopt the U-Net architecture. Figure 3 (left) illustrates the architecture of LaMamba-Diff-S. In particular, we follow LDMs with LaMamba-Diff operating in the latent space of the pre-trained VAE provided by Stable Diffusion¹ [41], which has a down-sampling factor of 8.

Input tokens. The input of LaMamba-Diff consists of timestep t , class label l , and noisy latent $z_t \in \mathbb{R}^{\frac{H}{8} \times \frac{W}{8} \times 4}$, which has the same dimensions as the latent of the pre-trained VAE. By viewing z_t as a $\frac{H}{8} \times \frac{W}{8}$ grid of features, we treat every position on the grid as a patch (i.e., 1×1 patch size) and linearly embed every patch without the need to flatten it into a 1-D sequence. This encodes z_t into a latent representation of size $\frac{H}{8} \times \frac{W}{8} \times D$, where D is the hidden dimension. Meanwhile, t and l are encoded into continuous representations using an MLP and a learnable embedding dictionary, respectively; the sum of these two encoding results becomes the conditioning embedding c .

U-Net architecture. As illustrated in Fig. 3 (left), LaMamba-Diff consists of an encoder, a bottleneck stage, and a decoder, with skip connections between corresponding stages of the encoder and decoder. Skip connections are implemented with channel-wise addition instead of channel concatenation. Under similar number of parameters and computational cost (GFLOPs), skip connections with chan-

nel concatenation result in a smaller number of hidden dimensions, which can lead to sub-optimal performance as shown in the ablation study presented in Table 7. Hierarchical representations are built by downsampling feature maps from stages 1 and 2 of the encoder with patch merging [31], and upsampling feature maps fed into stages 1 and 2 of the decoder with patch expansion [6]. Thus, the spatial resolution at the bottleneck stage is 4 times smaller than the input resolution of the encoder.

Notably, we allow the propagation of fine-grained local information across window boundaries in local attention by applying an alternating shifting scheme [31] to every two consecutive blocks. Specifically, for every two blocks, the first block adopts the standard window partitioning scheme for local attention, while the second block adopts a windowing configuration that is shifted from the first block by $(\lfloor \frac{M}{2} \rfloor, \lfloor \frac{M}{2} \rfloor)$, where M represents the window size, which is set to 8 by default.

We design four distinct LaMamba-Diff models with different scales (Table 1), each having a comparable number of parameters to its corresponding DiT variant [37], allowing fair comparisons of the model architecture. The architecture overview has been presented in Section 4.2. The condition embedding dimensions for Small, Base, Large, and X-Large are 192, 384, 1024, and 1280 respectively. All LaMamba-Diff variants have two downsampling and upsampling blocks only in stages 1 and 2. Our large and X-large variants have four stages without extra downsampling and upsampling blocks.

Noise and covariance prediction. We apply AdaLN before linearly projecting and reshaping the output of the de-

¹<https://huggingface.co/stabilityai/sd-vae-ft-mse>

coder to predict noise ϵ and covariance Σ , which have the same dimensions as the input noisy latent z_t (i.e., $\epsilon, \Sigma \in \mathbb{R}^{\frac{H}{8} \times \frac{W}{8} \times 4}$).

Local detail preservation. Fine-grained local information within each patch is crucial for excavating features from visual data [18]. However, existing diffusion models based on Transformers (such as DiT [37]) and SSMs (such as DiffuSSM [55] and DiS [10]) do not effectively handle this aspect. When larger patch sizes are used, this limitation leads to a loss of local details and a corresponding increase in FID [37]. On the other hand, using smaller patch sizes results in an increased computational cost as the input sequence length is inversely proportional to the squared patch size. We prevent the loss of valuable fine-grained information by utilizing 1×1 patches, which is computationally feasible thanks to the linear complexity and efficient design of LaMamba-Diff.

4.3. Computational Complexity Analysis

In this section, we provide theoretical and empirical analysis of computational complexity for LaMamba-Diff. Since the selective scan 2D (SS2D) mechanism contributes to the majority of FLOPs in VSSM by computing 4 SSM processes with a hidden dimension expansion ratio of 2 [30], we approximate the complexity of VSSM with SS2D.

Given a noisy diffusion latent $z \in \mathbb{R}^{\frac{H}{8} \times \frac{W}{8} \times D}$, where D is the hidden dimension, the computational complexity of SS2D, windowed multi-head self-attention (W-MSA), and feedforward net (FFN) are given below:

$$\begin{aligned} \Omega(\text{SS2D}) &= 4\Omega(\text{SSM}) \\ &= 4(3L(2D)N + L(2D)N), \end{aligned} \quad (3)$$

$$\Omega(\text{W-MSA}) = 4HWD^2 + 2M^2HWD, \quad (4)$$

$$\Omega(\text{FFN}) = 4LD^2, \quad (5)$$

where $L = H \times W$ denotes the sequence length, N is the SSM state dimension that encodes the context of each channel independently, and M is the fixed window size. Since SS2D computes four SSM processes corresponding to four scan paths, its complexity can be approximated with $4\Omega(\text{SSM})$. For SSM, $3L(2D)N$ comes from the computation of \bar{B} , C , and \bar{D} while the computation of \bar{A} contributes to the complexity of $L(2D)N$. As a result, the overall complexity of VSSM can be approximated as $\Omega(\text{SS2D})$, which is linear with respect to L . Given a window with fixed size $M = 8$, the complexity of W-MSA is linear with respect to sequence length. Hence, all three components of LaMamba, namely VSSM, local attention, and FFN, have linear complexity. Built upon LaMamba, LaMamba-Diff is naturally linear. We note that the following operations contribute negligible GFLOPs and are excluded from this analysis for simplicity: reshaping and merging the 4 SSM

Resolution	Model	Sequence length	# GFLOPs
256×256	DiT-XL/2	256	118.64
	LaMamba-Diff-XL	1024	50.46
512×512	DiT-XL/2	1024	524.60
	LaMamba-Diff-XL	4096	201.20
1024×1024	DiT-XL/2	4096	2910.30
	LaMamba-Diff-XL	16384	804.18

Table 2. Comparison of GFLOPs between LaMamba-Diff-XL and DiT-XL/2 for different image resolutions.

outputs in SS2D; AdaLN and scaling multiplications with α in LaMamba blocks.

Empirically, we compare GFLOPs of LaMamba-Diff-XL with DiT-XL/2 for different image resolutions in Table 4.3. With a comparable number of parameters, LaMamba-Diff-XL incurs 57.5% and 72.4% less GFLOPs at 256×256 and 1024×1024 resolutions, respectively. Notably, LaMamba-Diff’s U-Net architecture decreases computational complexity by downsampling the input sequence with patch merging in two encoder stages.

5. Experiments

5.1. Setting

Latent diffusion model. For all experiments, LaMamba-Diff operates in the latent space of an off-the-shelf pre-trained VAE ² from Stable Diffusion [41], which has a downsampling factor of 8. For instance, an RGB image x_0 of size $256 \times 256 \times 3$ would be encoded into a compressed latent $z_0 = \mathcal{E}(x_0)$ of size $32 \times 32 \times 4$. Our LaMamba-Diff is trained to learn the reverse diffusion process in this \mathcal{Z} -space using diffusion hyperparameters from ADM [8]. Specifically, we follow their embedding approach to encode timestep and class label conditions, and use a linear variance scheduler and ADM’s parameterization of covariance Σ_θ . Images are generated by sampling novel latents z and passing them to the VAE decoder $x = \mathcal{D}(z)$.

Training Details. We follow the training and hyperparameter settings in [37] to train variants of LaMamba-Diff on the ImageNet dataset [44] at 256×256 and 512×512 resolutions using classifier free guidance [20]. Specifically, we utilize the weight initialization techniques in [37] and employ the AdamW optimizer [32] with a constant learning rate of $1e-4$, a global batch size of 256, and no weight decay. An exponential moving average (EMA) of LaMamba-Diff weights is maintained during training with a decay of 0.9999. We follow the setting in [30] for VSSM hyperparameters.

Evaluation. We measure model performance with Fréchet Inception Distance (FID) [19], a standard metric for assessing the quality of generated images. For a fair compari-

²<https://huggingface.co/stabilityai/sd-vae-ft-mse>

ImageNet 256×256									
Model	Parameters(M)	GFLOPs	Training Steps(M)	FID↓	sFID↓	IS↑	Precision↑	Recall↑	
Model Size	5								
Steps	48								
Unconditional									
ADM [8]	554	1120	2.0	10.94	6.02	100.98	0.69	0.63	
ADM-U [8]	608	742	2.0	7.49	5.13	127.49	0.72	0.63	
LDM-8 [41]	395	79	1.2	15.51	-	79.03	0.65	0.63	
LDM-4 [41]	391	103	0.8	10.56	-	103.49	0.71	0.62	
DiT-XL/2 [37]	675	118	7.0	9.62	6.85	121.50	0.67	0.67	
DiffuSSM-XL [55]	673	280	2.6	9.07	5.52	118.32	0.69	0.64	
LaMamba-Diff-XL	656	50	2.0	6.12	5.58	149.13	0.71	0.64	
Classifier-free guidance									
ADM-G, ADM-U [8]	673	761	2.0	3.94	6.14	215.84	0.83	0.53	
LDM-8-G [41]	395	79	1.2	7.76	-	209.52	0.84	0.35	
LDM-4-G [41]	391	103	0.8	3.60	-	247.67	0.87	0.48	
U-ViT-H/2-G [3]	501	133	2.0	2.29	-	247.67	0.87	0.48	
DiffuSSM-XL-G [55]	673	280	2.6	2.28	4.49	259.13	0.86	0.56	
DiT-XL/2-G [37]	675	118	7.0	2.27	4.60	278.24	0.83	0.57	
LaMamba-Diff-XL-G	656	50	2.0	2.04	4.52	296.07	0.84	0.56	
ImageNet 512×512									
Unconditional									
DiT-XL/2 [37]	675	524	3.0	12.03	7.12	105.25	0.75	0.64	
LaMamba-Diff-XL	656	201	3.0	7.76	6.89	122.41	0.81	0.60	
Classifier-free guidance									
ADM-G, ADM-U [8]	774	2834	1.9	3.85	5.86	221.72	0.84	0.53	
U-ViT-H/4-G [3]	501	133	2.0	4.05	8.44	261.13	0.84	0.48	
DiffuSSM-XL-G [55]	673	1066	1.2	3.41	5.84	255.06	0.85	0.49	
DiT-XL/2-G [37]	675	524	3.0	3.04	5.02	240.82	0.84	0.54	
LaMamba-Diff-XL-G	656	201	3.0	3.01	5.15	277.19	0.85	0.52	

Table 3. **Quantitative comparison of image generation quality on ImageNet 256x256 and 512x512.** We denote classifier-free guidance by appending "-G" to model names. LaMamba-Diff-XL achieves competitive performance with substantially fewer GFLOPs. The training steps denote the number of iterations trained using a batch size of 256.

son with prior works, we use 250 DDPM sampling steps to sample 50K images to compute FID [37] using the ADM’s TensorFlow implementation [8]. We also report sFID [33], Inception Score [46], and Precision and Recall [27] as secondary performance metrics.

5.2. Main Results

ImageNet 256x256. We compare our largest model, LaMamba-Diff-XL trained for 2M steps, with state-of-the-art (SOTA) diffusion models on ImageNet at 256x256 resolution. Table 3 reports quantitative performance evaluation results, while qualitative examples are provided in Figures 4-9. In both unconditional and class-conditional settings, LaMamba-Diff-XL outperforms attention-only (DiT [37], U-ViT [3]) and SSM-only (DiffuSSM [55]) methods, achieving clearly lower FID scores. More importantly, LaMamba-Diff-XL achieves SOTA FIDs while requiring substantially fewer GFLOPs. In unconditional im-

age generation, LaMamba-Diff-XL achieves a SOTA FID of 6.12, improving the previous SOTA FID (9.07) by 2.95 (33%) with 82% fewer GFLOPs and 17M fewer parameters. Furthermore, LaMamba-Diff-XL achieves the highest Inception Score (IS) and Precision. In conditional image generation with classifier-free guidance (CFG) [20], LaMamba-Diff-XL achieves a SOTA FID of 2.04 using 57.6% fewer GFLOPs and 19M fewer parameters compared to DiT-XL/2. Moreover, LaMamba-Diff-XL achieves the highest Inception Score of 296.07. Note that the previous SOTA conditional FID of 2.10 was achieved by DiS-H/2 [10] (900M), and LaMamba-Diff-XL uses 27% fewer parameters and needs 77% fewer GFLOPs.

ImageNet 512x512. We evaluate the image generation quality of LaMamba-Diff-XL on ImageNet at 512x512 resolution. Here, LaMamba-Diff-XL processes 4096 tokens with an input latent of size $64 \times 64 \times 4$. Table 3 shows comparisons with SOTA methods, while Figures 10-15 ex-

Model	Parameters (M)	GFLOPs	FID
LaMamba-Diff-S	32	3.19	55.68
LaMamba-Diff-B	127	12.32	29.71
LaMamba-Diff-L	449	33.39	18.15
LaMamba-Diff-XL	656	49.90	12.86
DiT-S/2	33	6.06	68.40
DiT-B/2	130	23.01	43.47
DiT-L/2	458	80.71	23.33
DiT-XL/2	675	118.64	19.47

Table 4. Comparison of LaMamba-Diff and DiT scaling properties based on unconditional FID and models trained on ImageNet 256x256 for 400k steps using a batch size 256.

hibits examples of generated images. LaMamba-Diff-XL achieves lower FID compared to all prior diffusion models with similar sizes and uses 61.6% less GFLOPs compared to DiT-XL/2. In the unconditional setting, LaMamba-Diff-XL substantially improves the FID of DiT-XL/2 from 12.03 to 7.76. When using classifier-free guidance, LaMamba-Diff-XL achieves a SOTA FID of 3.01 and the highest IS of 277.19. Note that DiS-H/2 [10] achieves a slightly lower FID (2.88) using 37% more parameters and 258% more GFLOPs. These results highlight the capability and efficiency of LaMamba-Diff in high-resolution image generation.

Scaling model complexity Here we evaluate the scaling properties of LaMamba-Diff by training the four models presented in Table 4.2 on ImageNet 256x256 for 400k steps using the same hyperparameters. Figure 2 (left) and Table 4 present our results. We observe substantial FID improvements when increasing the number of parameters. In comparison to LaMamba-Diff-S with 32M parameters, LaMamba-Diff-XL with 656M parameters improves the FID score by 42.82. LaMamba-Diff models outperform DiT models with a comparable number of parameters by consistently exhibiting superior performance while using significantly fewer GFLOPs. These observations underscore the superior scaling capability of LaMamba-Diff models.

5.3. Ablation studies

In this section, we investigate the effectiveness of each proposed component in our LaMamba block as well as in the overall network architecture. Unless otherwise stated, we report FID-50K for variants of LaMamba-Diff Tiny trained on ImageNet 256x256 for 400K steps with a batch size of 256.

Local attention. The local attention in our LaMamba block is crucial to success, complementing VSSM by capturing detailed local contextual information. In Table 5, we study the effect of local attention and different atten-

Method	GFLOPs	FID
LaMamba-Diff	3.19	55.68
w/o attention	2.45	69.78
w/o shifting	3.19	58.81
global attention	4.24	53.74

Table 5. Ablation study of attention in LaMamba blocks.

Method	Parameters (M)	GFLOPs	FID
LaMamba-Diff	32	3.19	55.68
SS2D [30]	32	3.19	56.57
Bi-directional Mamba [58]	30	2.62	83.99
LocalVMamba [23]	32	3.32	92.10
EfficientVMamba [38]	31	2.40	105.93

Table 6. Ablation study of VSSM in LaMamba blocks.

tion strategies. Specifically, we removed the local attention module entirely (w/o attention) or disabled the alternating window shift (w/o shifting). Additionally, we replaced local attention with global attention.

Table 5 presents our results, indicating that removing local attention leads to a substantial increase in FID by 14.1, confirming the importance of modeling detailed local contexts. Additionally, removing the shifting scheme for windowed attention leads to a 3.13 increase in FID, suggesting that the propagation of fine-grained information across window boundaries is useful. Global attention marginally improves FID by 3.5 despite bringing a significant 32.5% computational overhead, indicating that the combination of local attention and VSSM is as powerful as global attention plus VSSM in capturing both global and local contexts while incurring much less computation.

Visual state space module (VSSM). In LaMamba blocks, VSSM is responsible for capturing global contexts and 2D spatial information from inputs. Here, we explore the performance of different VSSMs discussed in Section 4.1. We follow the original implementation and Mamba hyperparameters released in the corresponding GitHub repositories. As demonstrated in Table 6, LaMamba-Diff with spatially continuous SS2D achieves superior performance, and spatially continuous scanning [56] improves FID by 0.89. Under comparable numbers of parameters, SS2D outperforms other VSSM variants significantly, thereby highlighting its effectiveness in capturing global contexts in latent diffusion models.

Network architecture. In this section, we conduct a comparative analysis of various architectural design choices. Specifically, we evaluate four types of architectural variations: the adoption of an isotropic architecture instead of a U-Net architecture, the number of downsampling blocks in U-Net, the number of LaMamba blocks in each U-Net stage, and the adoption of channel concatena-

Ablation Type	Method	Initial hidden dim	Parameters (M)	GFLOPs	FID
	LaMamba-Diff	96	32	3.19	55.68
Downsampling	1x	144	30	6.99	53.49
	3x	48	33	1.93	62.23
Block Number	Decoder -1	104	32	3.08	54.93
	All +1	80	33	3.51	63.54
	All -1	112	35	2.93	58.17
Isotropic architecture	Patch size 1	384	34	24.96	52.01
	Patch size 2	384	34	6.19	91.89
	Patch size 4	384	34	1.96	129.92
	Patch size 8	384	34	0.65	172.10
U-Net Shortcut	Concatenate	64	33	3.02	89.10

Table 7. Ablation studies on architectural design choices.

tion instead of addition in U-Net shortcuts. The hidden dimension is adjusted to ensure that all architectural variants considered in the same comparison have a similar number of parameters. The results of these ablations are presented in Table 7.

In LaMamba-Diff, we downsample twice, resulting in a bottleneck resolution of 8×8 for 256×256 input images. Here, we investigate the impact of downsampling only once ($1 \times$) and three times ($3 \times$), corresponding to bottleneck resolutions of 16×16 and 4×4 , respectively. Our observations reveal that $3 \times$ downsampling leads to a decline in performance, while $1 \times$ downsampling marginally improves FID by 3.9, albeit with an 118% increase in GFLOPs.

Next, we analyze the effect of varying the number of LaMamba blocks in each stage of the encoder and decoder in LaMamba-Diff, where each encoder stage has 2 blocks and each decoder stage has 3 blocks. We assess performance variations by using 2 blocks only in every decoder stage (Decoder -1), adding one block to every stage in both encoder and decoder (All +1), or removing one block from every stage in both encoder and decoder (All -1). Our results indicate that increasing the number of blocks in every stage at the cost of decreasing hidden dimensions leads to performance drops. Moreover, using less LaMamba blocks in the decoder (Decoder -1) achieves comparable FID and GFLOPs, providing an alternative architectural design for LaMamba-Diff, which nevertheless, adopts the decoder design in StableDiffusion [41] to make it stronger.

We also compare LaMamba-Diff with an isotropic architecture with no downsampling, which is essentially a DiT [37] with LaMamba blocks. We observe that an isotropic architecture using a patch size of 1 can marginally improve FID by 3.67 at the cost of 7.8 times more GFLOPs, while larger patch sizes result in inferior performance. In contrast, our U-Net architecture presents a significantly superior trade-off between FID and GFLOPs.

Compared to channel concatenation in U-Net short-

cuts [41], LaMamba-Diff achieves substantially lower FID with a comparable number of parameters and a larger hidden dimension of 96. Overall, architecture ablation studies suggest that the size of hidden dimensions is crucial to the success of LaMamba-Diff.

6. Conclusion

In this paper, we have proposed LaMamba-Diff, a novel linear-time backbone network for diffusion models. It efficiently captures both global contexts and local dependencies from input tokens. Our experiments demonstrate that LaMamba-Diff, with comparable number of parameters and significantly fewer GFLOPs, achieves very competitive performance against state-of-the-art diffusion backbones. Furthermore, our LaMamba block demonstrates excellent scalability, and like DiT, can be taken as a generic building block for various types of diffusion models, including both text-to-image and text-to-video diffusion models.

References

- [1] Md Atik Ahamed and Qiang Cheng. Mambatab: A simple yet effective approach for handling tabular data. *arXiv preprint arXiv:2401.08867*, 2024. 3
- [2] Jimmy Lei Ba, Jamie Ryan Kiros, and Geoffrey E Hinton. Layer normalization. *arXiv preprint arXiv:1607.06450*, 2016. 4, 5
- [3] Fan Bao, Shen Nie, Kaiwen Xue, Yue Cao, Chongxuan Li, Hang Su, and Jun Zhu. All are worth words: A vit backbone for diffusion models. In *Proceedings of the IEEE/CVF Conference on Computer Vision and Pattern Recognition*, pages 22669–22679, 2023. 8
- [4] Fan Bao, Shen Nie, Kaiwen Xue, Chongxuan Li, Shi Pu, Yaole Wang, Gang Yue, Yue Cao, Hang Su, and Jun Zhu. One transformer fits all distributions in multi-modal diffusion at scale. In *International Conference on Machine Learning*, pages 1692–1717. PMLR, 2023. 6
- [5] Andrew Brock, Jeff Donahue, and Karen Simonyan. Large

- scale gan training for high fidelity natural image synthesis. *arXiv preprint arXiv:1809.11096*, 2018. 8
- [6] Hu Cao, Yueyue Wang, Joy Chen, Dongsheng Jiang, Xiaopeng Zhang, Qi Tian, and Manning Wang. Swin-UNET: Unet-like pure transformer for medical image segmentation. In *European conference on computer vision*, pages 205–218. Springer, 2022. 6
- [7] Huiwen Chang, Han Zhang, Jarred Barber, AJ Maschinot, Jose Lezama, Lu Jiang, Ming-Hsuan Yang, Kevin Murphy, William T Freeman, Michael Rubinstein, et al. Muse: Text-to-image generation via masked generative transformers. *arXiv preprint arXiv:2301.00704*, 2023. 3
- [8] Prafulla Dhariwal and Alexander Nichol. Diffusion models beat gans on image synthesis. *Advances in neural information processing systems*, 34:8780–8794, 2021. 1, 4, 5, 7, 8
- [9] Patrick Esser, Robin Rombach, and Bjorn Ommer. Taming transformers for high-resolution image synthesis. In *Proceedings of the IEEE/CVF conference on computer vision and pattern recognition*, pages 12873–12883, 2021. 3
- [10] Zhengcong Fei, Mingyuan Fan, Changqian Yu, and Junshi Huang. Scalable diffusion models with state space backbone. *arXiv preprint arXiv:2402.05608*, 2024. 3, 4, 7, 8, 9
- [11] Yu Gao, Jiancheng Huang, Xiaopeng Sun, Zequn Jie, Yujie Zhong, and Lin Ma. Matten: Video generation with mamba-attention. *arXiv preprint arXiv:2405.03025*, 2024. 3
- [12] Ian Goodfellow, Jean Pouget-Abadie, Mehdi Mirza, Bing Xu, David Warde-Farley, Sherjil Ozair, Aaron Courville, and Yoshua Bengio. Generative adversarial nets. *Advances in neural information processing systems*, 27, 2014. 1, 3
- [13] Priya Goyal, Piotr Dollár, Ross Girshick, Pieter Noordhuis, Lukasz Wesolowski, Aapo Kyrola, Andrew Tulloch, Yangqing Jia, and Kaiming He. Accurate, large mini-batch sgd: Training imagenet in 1 hour. *arXiv preprint arXiv:1706.02677*, 2017. 4
- [14] Albert Gu and Tri Dao. Mamba: Linear-time sequence modeling with selective state spaces. *arXiv preprint arXiv:2312.00752*, 2023. 2, 3, 4, 5
- [15] Albert Gu, Karan Goel, and Christopher Ré. Efficiently modeling long sequences with structured state spaces. *arXiv preprint arXiv:2111.00396*, 2021.
- [16] Albert Gu, Isys Johnson, Karan Goel, Khaled Saab, Tri Dao, Atri Rudra, and Christopher Ré. Combining recurrent, convolutional, and continuous-time models with linear state space layers. *Advances in neural information processing systems*, 34:572–585, 2021. 3
- [17] Ankit Gupta, Albert Gu, and Jonathan Berant. Diagonal state spaces are as effective as structured state spaces. *Advances in Neural Information Processing Systems*, 35:22982–22994, 2022. 4
- [18] Kai Han, An Xiao, Enhua Wu, Jianyuan Guo, Chunjing Xu, and Yunhe Wang. Transformer in transformer. *Advances in neural information processing systems*, 34:15908–15919, 2021. 2, 3, 7
- [19] Martin Heusel, Hubert Ramsauer, Thomas Unterthiner, Bernhard Nessler, and Sepp Hochreiter. Gans trained by a two time-scale update rule converge to a local nash equilibrium. *Advances in neural information processing systems*, 30, 2017. 7
- [20] Jonathan Ho and Tim Salimans. Classifier-free diffusion guidance. *arXiv preprint arXiv:2207.12598*, 2022. 2, 7, 8
- [21] Jonathan Ho, Ajay Jain, and Pieter Abbeel. Denoising diffusion probabilistic models. *Advances in neural information processing systems*, 33:6840–6851, 2020. 1, 2, 3, 5, 6
- [22] Vincent Tao Hu, Stefan Andreas Baumann, Ming Gui, Olga Grebenkova, Pingchuan Ma, Johannes Fischer, and Bjorn Ommer. Zigma: Zigzag mamba diffusion model. *arXiv preprint arXiv:2403.13802*, 2024. 3
- [23] Tao Huang, Xiaohuan Pei, Shan You, Fei Wang, Chen Qian, and Chang Xu. Localmamba: Visual state space model with windowed selective scan. *arXiv preprint arXiv:2403.09338*, 2024. 4, 9
- [24] Allan Jabri, David Fleet, and Ting Chen. Scalable adaptive computation for iterative generation. *arXiv preprint arXiv:2212.11972*, 2022. 2
- [25] Tero Karras, Miika Aittala, Timo Aila, and Samuli Laine. Elucidating the design space of diffusion-based generative models. *Advances in Neural Information Processing Systems*, 35:26565–26577, 2022. 2
- [26] Diederik P Kingma and Max Welling. Auto-encoding variational bayes. *arXiv preprint arXiv:1312.6114*, 2013. 3
- [27] Tuomas Kynkäänniemi, Tero Karras, Samuli Laine, Jaakko Lehtinen, and Timo Aila. Improved precision and recall metric for assessing generative models. *Advances in neural information processing systems*, 32, 2019. 8
- [28] Jiarun Liu, Hao Yang, Hong-Yu Zhou, Yan Xi, Lequan Yu, Yizhou Yu, Yong Liang, Guangming Shi, Shaoting Zhang, Hairong Zheng, et al. Swin-umamba: Mamba-based unet with imagenet-based pretraining. *arXiv preprint arXiv:2402.03302*, 2024. 2, 3
- [29] Jiuming Liu, Ruiji Yu, Yian Wang, Yu Zheng, Tianchen Deng, Weicai Ye, and Hesheng Wang. Point mamba: A novel point cloud backbone based on state space model with octree-based ordering strategy. *arXiv preprint arXiv:2403.06467*, 2024. 2, 3
- [30] Yue Liu, Yunjie Tian, Yuzhong Zhao, Hongtian Yu, Lingxi Xie, Yaowei Wang, Qixiang Ye, and Yunfan Liu. Vmamba: Visual state space model. *arXiv preprint arXiv:2401.10166*, 2024. 2, 3, 4, 5, 7, 9
- [31] Ze Liu, Yutong Lin, Yue Cao, Han Hu, Yixuan Wei, Zheng Zhang, Stephen Lin, and Baining Guo. Swin transformer: Hierarchical vision transformer using shifted windows. In *Proceedings of the IEEE/CVF international conference on computer vision*, pages 10012–10022, 2021. 5, 6
- [32] Ilya Loshchilov and Frank Hutter. Decoupled weight decay regularization. *arXiv preprint arXiv:1711.05101*, 2017. 7
- [33] Charlie Nash, Jacob Menick, Sander Dieleman, and Peter W Battaglia. Generating images with sparse representations. *arXiv preprint arXiv:2103.03841*, 2021. 8
- [34] Alex Nichol, Prafulla Dhariwal, Aditya Ramesh, Pranav Shyam, Pamela Mishkin, Bob McGrew, Ilya Sutskever, and Mark Chen. Glide: Towards photorealistic image generation and editing with text-guided diffusion models. *arXiv preprint arXiv:2112.10741*, 2021. 1
- [35] Alexander Quinn Nichol and Prafulla Dhariwal. Improved denoising diffusion probabilistic models. In *International*

- Conference on Machine Learning*, pages 8162–8171. PMLR, 2021. [3](#)
- [36] Yuta Oshima, Shohei Taniguchi, Masahiro Suzuki, and Yutaka Matsuo. Ssm meets video diffusion models: Efficient video generation with structured state spaces. *arXiv preprint arXiv:2403.07711*, 2024. [3](#)
- [37] William Peebles and Saining Xie. Scalable diffusion models with transformers. In *Proceedings of the IEEE/CVF International Conference on Computer Vision*, pages 4195–4205, 2023. [2](#), [3](#), [4](#), [5](#), [6](#), [7](#), [8](#), [10](#)
- [38] Xiaohuan Pei, Tao Huang, and Chang Xu. Efficientvmamba: Atrous selective scan for light weight visual mamba. *arXiv preprint arXiv:2403.09977*, 2024. [4](#), [9](#)
- [39] Aditya Ramesh, Mikhail Pavlov, Gabriel Goh, Scott Gray, Chelsea Voss, Alec Radford, Mark Chen, and Ilya Sutskever. Zero-shot text-to-image generation. In *International Conference on Machine Learning*, pages 8821–8831. PMLR, 2021. [1](#), [3](#)
- [40] Aditya Ramesh, Prafulla Dhariwal, Alex Nichol, Casey Chu, and Mark Chen. Hierarchical text-conditional image generation with clip latents. *arXiv preprint arXiv:2204.06125*, 1(2):3, 2022.
- [41] Robin Rombach, Andreas Blattmann, Dominik Lorenz, Patrick Esser, and Björn Ommer. High-resolution image synthesis with latent diffusion models. In *Proceedings of the IEEE/CVF conference on computer vision and pattern recognition*, pages 10684–10695, 2022. [1](#), [2](#), [3](#), [4](#), [5](#), [6](#), [7](#), [8](#), [10](#)
- [42] Olaf Ronneberger, Philipp Fischer, and Thomas Brox. U-net: Convolutional networks for biomedical image segmentation. In *Medical image computing and computer-assisted intervention—MICCAI 2015: 18th international conference, Munich, Germany, October 5-9, 2015, proceedings, part III 18*, pages 234–241. Springer, 2015. [2](#), [6](#)
- [43] Jiacheng Ruan and Suncheng Xiang. Vm-unet: Vision mamba unet for medical image segmentation. *arXiv preprint arXiv:2402.02491*, 2024. [2](#), [3](#)
- [44] Olga Russakovsky, Jia Deng, Hao Su, Jonathan Krause, Sanjeev Satheesh, Sean Ma, Zhiheng Huang, Andrej Karpathy, Aditya Khosla, Michael Bernstein, et al. Imagenet large scale visual recognition challenge. *International journal of computer vision*, 115:211–252, 2015. [7](#)
- [45] Chitwan Saharia, William Chan, Saurabh Saxena, Lala Li, Jay Whang, Emily L Denton, Kamyar Ghasemipour, Raphael Gontijo Lopes, Burcu Karagol Ayan, Tim Salimans, et al. Photorealistic text-to-image diffusion models with deep language understanding. *Advances in Neural Information Processing Systems*, 35:36479–36494, 2022. [1](#), [3](#)
- [46] Tim Salimans, Ian Goodfellow, Wojciech Zaremba, Vicki Cheung, Alec Radford, and Xi Chen. Improved techniques for training gans. *Advances in neural information processing systems*, 29, 2016. [8](#)
- [47] Saeed Saremi and Terrence J Sejnowski. Hierarchical model of natural images and the origin of scale invariance. *Proceedings of the National Academy of Sciences*, 110(8):3071–3076, 2013. [5](#)
- [48] Axel Sauer, Katja Schwarz, and Andreas Geiger. Stylegan-xl: Scaling stylegan to large diverse datasets. In *ACM SIGGRAPH 2022 conference proceedings*, pages 1–10, 2022. [8](#)
- [49] Jimmy TH Smith, Andrew Warrington, and Scott W Linderman. Simplified state space layers for sequence modeling. *arXiv preprint arXiv:2208.04933*, 2022. [3](#)
- [50] Jascha Sohl-Dickstein, Eric Weiss, Niru Maheswaranathan, and Surya Ganguli. Deep unsupervised learning using nonequilibrium thermodynamics. In *International conference on machine learning*, pages 2256–2265. PMLR, 2015. [3](#)
- [51] Jiaming Song, Chenlin Meng, and Stefano Ermon. Denoising diffusion implicit models. *arXiv preprint arXiv:2010.02502*, 2020. [2](#)
- [52] Yang Song and Stefano Ermon. Generative modeling by estimating gradients of the data distribution. *Advances in neural information processing systems*, 32, 2019. [1](#)
- [53] Yang Song, Jascha Sohl-Dickstein, Diederik P Kingma, Abhishek Kumar, Stefano Ermon, and Ben Poole. Score-based generative modeling through stochastic differential equations. *arXiv preprint arXiv:2011.13456*, 2020. [3](#)
- [54] Ashish Vaswani, Noam Shazeer, Niki Parmar, Jakob Uszkoreit, Llion Jones, Aidan N Gomez, Łukasz Kaiser, and Illia Polosukhin. Attention is all you need. *Advances in neural information processing systems*, 30, 2017. [2](#), [3](#)
- [55] Jing Nathan Yan, Jiatao Gu, and Alexander M Rush. Diffusion models without attention. *arXiv preprint arXiv:2311.18257*, 2023. [2](#), [3](#), [4](#), [7](#), [8](#)
- [56] Chenhongyi Yang, Zehui Chen, Miguel Espinosa, Linus Ericsson, Zhenyu Wang, Jiaming Liu, and Elliot J Crowley. Plainmamba: Improving non-hierarchical mamba in visual recognition. *arXiv preprint arXiv:2403.17695*, 2024. [4](#), [5](#), [9](#)
- [57] Ling Yang, Zhilong Zhang, Yang Song, Shenda Hong, Runsheng Xu, Yue Zhao, Wentao Zhang, Bin Cui, and Ming-Hsuan Yang. Diffusion models: A comprehensive survey of methods and applications. *ACM Computing Surveys*, 2022. [3](#)
- [58] Lianghui Zhu, Bencheng Liao, Qian Zhang, Xinlong Wang, Wenyu Liu, and Xinggang Wang. Vision mamba: Efficient visual representation learning with bidirectional state space model. *arXiv preprint arXiv:2401.09417*, 2024. [2](#), [3](#), [4](#), [9](#)

LaMamba-Diff: Linear-Time High-Fidelity Diffusion Models Based on Local Attention and Mamba

Supplementary Material

7. Additional Qualitative Results



Figure 4. ImageNet 256×256 samples generated by LaMamba-Diff-XL using a classifier-free guidance scale of 4.0.
Class: Ice Cream



Figure 5. ImageNet 256×256 samples generated by LaMamba-Diff-XL using a classifier-free guidance scale of 4.0.
Class: Tabby Cat



Figure 6. ImageNet 256×256 samples generated by LaMamba-Diff-XL using a classifier-free guidance scale of 2.0.
Class: Lakeshore



Figure 7. ImageNet 256×256 samples generated by LaMamba-Diff-XL using a classifier-free guidance scale of 2.0.
Class: Arctic Fox



Figure 8. ImageNet 256×256 samples generated by LaMamba-Diff-XL using a classifier-free guidance scale of 1.5.
Class: Macaw



Figure 9. ImageNet 256×256 samples generated by LaMamba-Diff-XL using a classifier-free guidance scale of 1.5.
Class: Greenhouse



Figure 10. ImageNet 512×512 samples generated by LaMamba-Diff-XL using a classifier-free guidance scale of 4.0.
Class: Macaw



Figure 11. ImageNet 512×512 samples generated by LaMamba-Diff-XL using a classifier-free guidance scale of 4.0.
Class: Ice Cream



Figure 12. ImageNet 512×512 samples generated by LaMamba-Diff-XL using a classifier-free guidance scale of 2.0.
Class: Sulphur-crested Cockatoo



Figure 13. ImageNet 512×512 samples generated by LaMamba-Diff-XL using a classifier-free guidance scale of 2.0.
Class: Tenco snowbird



Figure 14. ImageNet 512×512 samples generated by LaMamba-Diff-XL using a classifier-free guidance scale of 1.5.
Class: Husky

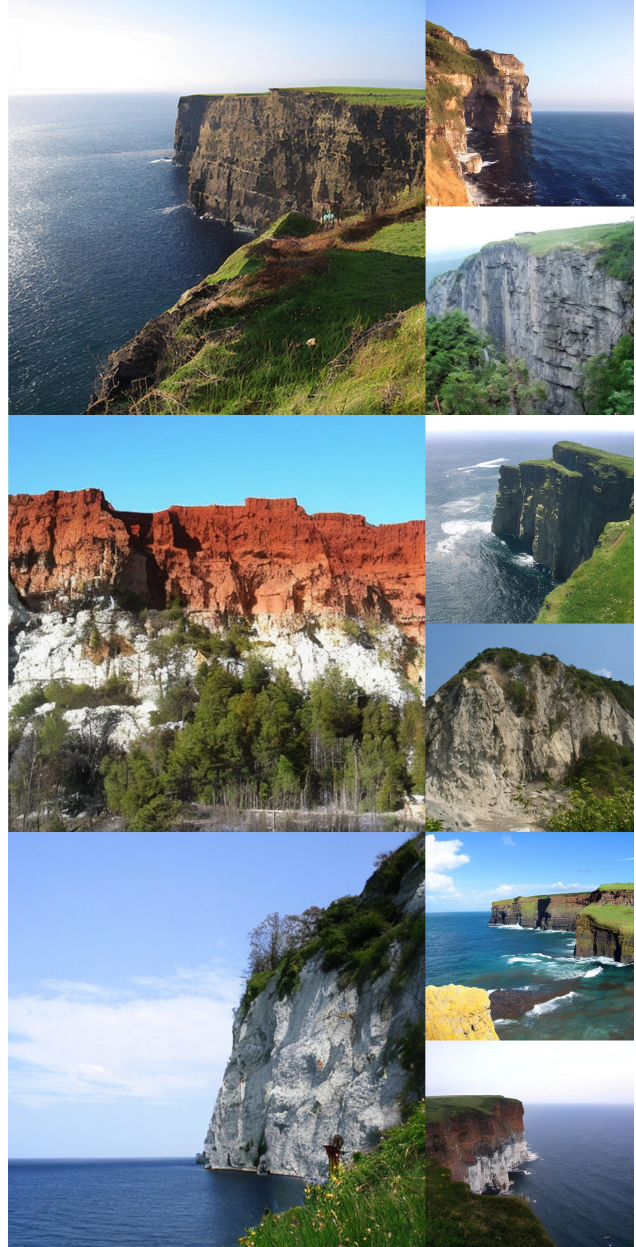


Figure 15. ImageNet 512×512 samples generated by LaMamba-Diff-XL using a classifier-free guidance scale of 1.5.
Class: Cliff